Journal of Computer-Aided Molecular Design (2018) 32:643–655
https://doi.org/10.1007/s10822-018-0118-x

Discovery of a small-molecule inhibitor of Dvl–CXXC5 interaction by computational approaches

Songling Ma[1,2] · Jiwon Choi[2] · Xuemei Jin[1] · Hyun-Yi Kim[3] · Ji-Hye Yun[4] · Weontae Lee[4] · Kang-Yell Choi[3] · Kyoung Tai No[1,2]

Received: 22 June 2017 / Accepted: 2 April 2018 / Published online: 7 April 2018

Abstract

The Wnt/β-catenin signaling pathway plays a significant role in the control of osteoblastogenesis and bone formation. CXXC finger protein 5 (CXXC5) has been recently identified as a negative feedback regulator of osteoblast differentiation through a specific interaction with Dishevelled (Dvl) protein. It was reported that targeting the Dvl–CXXC5 interaction could be a novel anabolic therapeutic target for osteoporosis. In this study, complex structure of Dvl PDZ domain and CXXC5 peptide was simulated with molecular dynamics (MD). Based on the structural analysis of binding modes of MD-simulated Dvl PDZ domain with CXXC5 peptide and crystal Dvl PDZ domain with synthetic peptide–ligands, we generated two different pharmacophore models and applied pharmacophore-based virtual screening to discover potent inhibitors of the Dvl–CXXC5 interaction for the anabolic therapy of osteoporosis. Analysis of 16 compounds selected by means of a virtual screening protocol yielded four compounds that effectively disrupted the Dvl–CXXC5 interaction in the fluorescence polarization assay. Potential compounds were validated by fluorescence spectroscopy and nuclear magnetic resonance. We successfully identified a highly potent inhibitor, BMD4722, which directly binds to the Dvl PDZ domain and disrupts the Dvl–CXXC5 interaction. Overall, CXXC5–Dvl PDZ domain complex based pharmacophore combined with various traditional and simple computational methods is a promising approach for the development of modulators targeting the Dvl–CXXC5 interaction, and the potent inhibitor BMD4722 could serve as a starting point to discover or design more potent and specific the Dvl–CXXC5 interaction disruptors.

Keywords Wnt/β-catenin signaling pathway · Dvl–CXXC5 interaction · Pharmacophore · Virtual screening · Molecular dynamics simulation · Nuclear magnetic resonance

Introduction

Osteoporosis is a common skeletal disorder characterized by low bone mass and microarchitectural deterioration of bone tissue, resulting in increased bone fragility and fracture risk [1]. Osteoporosis literally means porous bones, in which the balance between old bone resorption by osteoclasts and new bone formation by osteoblasts is disrupted. The interactions between resorption of old or damaged bone by osteoclasts and formation of new bone by osteoblasts are critical in regulation of bone remodeling.

The Wnt/β-catenin signaling pathway as a protein interaction network is a key regulator of cell proliferation and differentiation. Abnormal activation or inhibition of this signaling pathways has been implicated in cancer and many other human diseases, including fibrosis [2], metabolic disease [3], and neurodegenerative disorders [4, 5]. In bone

Songling Ma and Jiwon Choi are co-first authors.

Electronic supplementary material The online version of this article (https://doi.org/10.1007/s10822-018-0118-x) contains supplementary material, which is available to authorized users.

✉ Kyoung Tai No
ktno@bmdrc.org; ktno@yonsei.ac.kr

1 Department of Biotechnology, College of Life Science and Biotechnology, Yonsei University, Seoul 03722, Republic of Korea

2 Bioinformatics and Molecular Design Research Center, Yonsei University, Seoul 03722, Republic of Korea

3 Translational Research Center for Protein Function Control, Yonsei University, Seoul 03722, Republic of Korea

4 Department of Biochemistry, College of Life Science and Biotechnology, Yonsei University, Seoul 03722, Republic of Korea

biology, activation of the Wnt/β-catenin signaling pathway induces osteoblast differentiation and bone mineral density in both animal experiments and clinical examinations [1, 6, 7]. For instance, osteoporosis, as well as sclerosteosis and van Buchem disease, has been associated with aberrations in the Wnt/β-catenin signaling during osteogenesis. Many components and regulators of this pathway control bone development and homeostasis. Among them, Dickkopf-1 (DKK1) and sclerostin (scl) have emerged as negative regulators, confirming the strong link between Wnt/β-catenin signaling and bone homeostasis. Inhibition of DKK1 and Scl with their respective antibodies, increases bone formation, bone mineral density, and bone strength in various animal models, and these antibodies are currently being tested in clinical trials for the treatment of bone loss and for bone repair [8].

CXXC finger protein 5 (CXXC5) is a CXXC-type zinc finger family protein that was identified as a negative feedback regulator of the Wnt/β-catenin signaling pathway [9]. In the activated state of Wnt/β-catenin signaling pathway, Dishevelled (Dvl) protein dissociates the cytoplasmic β-catenin destruction complex that is constituted of Axin, adenomatous polyposis coli, glycogen synthase kinase 3β, and casein kinase 1, which results in β-catenin stabilization and nuclear translocation. In the nucleus, accumulated β-catenin interacts with co-transcriptional factors to activate the expression of target genes [7]. CXXC5, a target gene of Wnt/β-catenin pathway, is induced by activation of Wnt/β-catenin signaling pathway. Moreover, activation of this pathway enhances the interaction of CXXC5 with Dvl. The interaction of CXXC5 with Dvl blocks the dissociation of β-catenin destruction complex, ultimately leading to inhibition of the Wnt/β-catenin signaling pathway [10–12].

In our previous work [9], we have demonstrated that CXXC5 knock-out results in elevated bone mineral density and trabecular number in mice without any severe gross developmental abnormalities. A Dvl binding motif (DBM, **RKTGHQICKFRKC**) was identified in the C-terminal region of CXXC4/Idax and CXXC5, and disruption of the Dvl–CXXC5 interaction with the DBM peptide activated the Wnt/β-catenin signaling pathway, leading to enhanced differentiation of osteoblasts and accelerated thickness growth of ex vivo-cultured calvariae. These data suggest that the Dvl–CXXC5 interaction could represent an attractive therapeutic target for novel bone anabolic agents to treat diseases associated with bone loss [9]. Several small-molecule inhibitors have been developed to regulate the Wnt/β-catenin signaling pathway by directly interacting with the Dvl PDZ domain. PDZ crystal structures have been widely used to developed PDZ inhibitors and binders [13–16]. In previous publications, two H-bonds from the carboxyl group, as well as an adjacent hydrophobic group were key features of FJ9 (designed based on peptide ligand of PSD95-PDZ3) [17], NSC668036 (identified from Dvl PDZ structure-based ligand screening) [13], 3289–8625 (identified from Dapper peptide–Dvl PDZ complex based 3D distance constraints screening) [14, 15], KY-02061 (screened through in vitro assay system) and KY-02327 (synthesized KY-02061 analog) [18], and BMD4702 (identified from small molecules-Dvl PDZ interaction based pharmacophore virtual screening) [16] for Dvl PDZ domain binders.

During the discovery of BMD4702 [16], core pharmacophore features (three hydrogen bond acceptors, three hydrophobic features) were found to contribute to the high affinity of the interaction of BMD4702 and the Dvl PDZ domain. However, BMD4702 failed to interrupt the interaction of Dvl–CXXC5 (data not shown), although it showed high affinity for the Dvl PDZ domain. To identify novel non-peptide small-molecule inhibitors of the Dvl PDZ and CXXC5 protein–protein interaction (PPI), in this study, pharmacophore models were generated based on specific interaction features revealed by molecular dynamics (MD)-simulated DBM peptide–Dvl PDZ domain and binding features of known crystal synthetic peptide ligands–Dvl PDZ domain. After virtual screening, the 16 virtual hits were experimentally tested in an in vitro competitive binding assay and by biophysical methods. Finally, we confirmed that compound BMD4722 specifically binds with low micromolar affinities to the DBM peptide binding site in the Dvl PDZ domain by conducting nuclear magnetic resonance (NMR) chemical shift perturbation and saturation transfer difference (STD) NMR experiments.

Materials and methods

Molecular dynamics simulation

Dvl PDZ domain of X-ray complex structure (PDB ID: 3CBX) was extracted as the initial structure. The starting structure of Dapper peptide (**SLKLMTTV**) was derived from X-ray structure of complex (PDB ID: 1L6O), and that of DBM peptide was generated based on the Dapper peptide. The MD simulations of the Dvl–Dapper and Dvl–DBM complexes were performed by using the Desmond 4.1 implemented in Maestro program of Schrödinger (Schrödinger, New York, NY, 2017) [19–21]. The two simulations were studied using the OPLS_2005 force field in explicit solvent with the TIP3P model [22]. In both MD simulations, ions (Na^+ and Cl^-) were added to simulate physiological concentration of monovalent ions (0.15 M). NPT (constant number of particles, pressure, and temperature) employed constant temperature (300 K) and pressure (1.01325 bar) as ensemble class. The particle-mesh Ewald method [23] was applied to calculate long-range electrostatic interactions and a cutoff of 9 Å of was chosen for van der Waals and short-range electrostatic

interactions. Nose–Hoover thermostats [24] were utilized to keep the constant simulation temperature, and the Martina–Tobias–Klein method [25] was used to control the pressure. RESPA integrator [26] was employed in order to integrate the equations of motion with an inner time step of 2.0 fs for bonded interactions and non-bonded interactions within the short-range cutoff. To reach the equilibration of system, the default protocol in Desmond was used. After reaching the equilibrium, two separate MD simulations of were run during 50 ns and 100 ns, respectively, and the snapshot configurations were saved every 5 ps interval. Analyses were carried out by using root-mean-square deviation (RMSD) generated from Schrödinger. Plots of RMSD obtained from MD simulation were generated using Excel 2013, and structure figures were created with the PyMOL program [27].

Pharmacophore model development and virtual screening

Pharmacophore models were generated based on the X-ray crystal structures of the Dvl PDZ domain-synthetic peptides (3CBX (peptide–ligand: **GGGWKWYGF**), 3CBY (peptide–ligand: **KDYGWIDGK**), 3CC0 (peptide–ligand: **EIVLWSDIP**), and 1L6O) and simulated complex of the Dvl PDZ domain and DBM peptide by using the *Receptor-Ligand Pharmacophore Generation protocol* of Accelrys Discovery Studio v 4.1 (DS, Accelrys Inc., San Diego, CA, USA). Entire pharmacophoric features were collected from the structural analysis, and two combinations of the partial pharmacophore features were selected to build the pharmacophore models, Pharm A and Pharm B.

Pharm A consisted of four hydrophobic groups (HY 1, HY 2, HY 3, and HY 4) and three H-bond acceptors (HBA 1, HBA 2, and HBA 3), and Pharm B consisted of three hydrophobic groups (HY 1, HY 2, and HY 5), three H-bond acceptors (HBA 1, HBA 2, and HBA 3), and one H-bond donor (HBD). Exclusion volume, representing the areas where subtle steric (ligand-target) hindrance can occur, was incorporated to each pharmacophore model.

An in-house 3D database consisting of approximately 8.0 million molecules was built by integrating of various commercial libraries. The 3D database was filtered by the pharmacophore models to screen virtual hits that could fit into the binding pocket of the Dvl PDZ domain with the Catalyst™ software package (DS). The filtered compounds were sorted by fit value, Lipinski's rule of five, and ADMET properties. Through cluster analysis, the compounds were grouped on the basis of their structural similarities. Eventually, 16 virtual hits were selected for further evaluation after visual inspection.

Competitive binding assay

In the fluorescence polarization assay [9], the purified Dvl PDZ domain (100 μL of 5 mg/mL) was added into each well of a 96-well Maxibinding Immunoplate (SPL, Seoul, Korea) and incubated overnight at 4 °C chamber. After washing with PBS, 100 μL of 10 μM PolyR-DBM tagged with fluorescein isothiocyanate was added into each well, and incubated for 4 h at 4 °C. After washing with PBS 3 times, 100 μL of different concentrations of small-molecule compounds in PBS was added into each well and incubated for 4 h at room temperature. The residual protein–peptide complex was examined by measuring the fluorescence intensity of each well using a Fluorstar Optima microplate reader (BGM Lab Technologie, Ortenberg, Germany).

Fluorescence spectroscopy experiment

An LS 55 fluorescence spectrophotometer was used to measure the binding affinities between compounds and the Dvl PDZ domain by using 280 nm excitation and 300–450 nm emission wavelengths. This assay was conducted in 100 mM potassium phosphate (pH 7.5), 0.5 mM EDTA, 2 mM DTT, and compounds, and titrated with 20 μM concentrated Dvl PDZ protein up to a molar ratio of 1:15 using a thermostat cuvette. Equation 1 was used to calculate the K_D value of the Dvl PDZ-compound complex,

$$\log[(F_0 - F)/F] = \log(1/K_D) + n \log[\text{ligand}] \quad (1)$$

where F_0 and F represent the fluorescence intensities of the protein at 360 nm in the absence and presence of compound, respectively. 'n' is the average number of binding sites per mole of protein.

NMR chemical shift perturbation experiment

For NMR titration, ^{1}H–^{15}N-HSQC experiment was performed at various molar ratios of (1:0, 1:10, 1:20, and 1:30) of ^{15}N-labeled Dvl PDZ domain to BMD4722. All NMR titration spectra were processed using TopSpin 3.1 (Bruker Biospin Corp., Billerica, MA, USA) and the NMR Pipe/NMRDraw software. Residues were completely assigned in each spectrum using Sparky program, and the following Eq. 2 was used to calculate chemical shift perturbations.

$$\Delta\delta_{AV} = \left((\Delta\delta_{1H})^2 + (\Delta\delta_{15N}/5)^2\right)^{1/2} \quad (2)$$

where $\Delta\delta_{AV}$, $\Delta\delta_1{}^H$, and $\Delta\delta_1{}^5{}_{/N}$ are the average, proton, and ^{15}N chemical shift changes respectively.

STD NMR experiment

STD NMR spectra were acquired at 298 K on an Avance 600 MHz spectrometer equipped with a 5 mm TXI Cryo-Probe. The concentrations of the BMD4722 and Dvl PDZ domain were fixed at 5 and 0.1 mM, respectively. Protein saturation was achieved using the STDDIFFESGP pulse. The on-resonance was set at − 600 Hz (− 1 ppm) and off resonance was set at 18,000 Hz (30 ppm), the saturation time was 3 s. 32 scans were acquired with 2 s relaxation delay between the scans. The data was processed using nmrPipe and plotted using the iNMR program. STD spectrum (I_{STD}) was obtained by subtracting on-resonance (I_{SAT}; protein saturation state) from off-resonance (I_0; protein unsaturation state).

Docking study

To determine the mode of the BMD4722 binding to the Dvl PDZ domain, molecular docking calculations were carried out using the CHARMm-based CDOCKER algorithm of DS, which uses a grid-based molecular docking method and samples initial ligand conformations via high-temperature molecular dynamics. The Dvl PDZ domain used for docking was derived from the 3CBX crystal complex structure. All of the generated binding poses were evaluated by calculating their binding energies using the *Calculate Binding Energies* protocol and then ranked accordingly. The predicted ligand complex structures were visualized using the PyMOL program.

Results

MD simulations of Dvl PDZ domain with DBM

To identify the specific binding pattern of Dvl and CXXC5 complex, two MD simulations were implemented with Desmond MD in Schrödinger to dock DBM peptide into the peptide-binding pocket of the Dvl PDZ domain for separated 50 and 100 ns, referenced by an MD simulation of Dapper peptide bound to the Dvl PDZ domain. RMSD in each trajectory structure was calculated with the initial structures as reference. Figure 1a shows that both simulations of DBM-bound Dvl PDZ domain and Dapper-bound Dvl PDZ domain reached stable equilibrium at around 30 ns of time and at around 2 Å of backbone RMSD in the same. It cross validated simulation process of peptides and implied the stability of backbone PDZ structures during simulations. Additionally, sidechain RMSD values at stable equilibrium were higher than that of backbone PDZ structure (Fig. 1b, c), demonstrating that binding of peptide did not induce structural change of PDZ backbone, while sidechains contributed peptide binding rather than PDZ backbone structure. The DBM peptide stayed in the binding pocket of Dvl PDZ domain during the simulation, as shown in the movie of snapshot configurations provided in supplementary file. The additional separated MD simulations lasting 50 ns was performed to collect more MD conformation samplings. Ten clusters of conformations were obtained by grouping similar RMSD values, and most appropriate structure from their RMSD matrix analyses were picked out in each cluster. The conformation, whose binding mode was most consistent with an $^{1}H–^{15}N$-HSQC NMR experiment described previously [18], was selected as simulated Dvl PDZ–DBM peptide complex.

The simulated DBM peptide interacted with Ser268, Ile269, and Val270 of the βB sheet, and Leu324, Arg325, and Val328 of the αB helix of Dvl PDZ domain binding pocket (Fig. 2a). Comparing the binding mode of simulated DBM peptide bound to Dvl PDZ domain with that of crystal synthetic peptides (3CBX, 3CC0) revealed that the three peptide ligands adopt similar conformations when bound to the PDZ domain, rather than that of Dapper peptide (Fig. 2b–d).

Structure-based pharmacophore model generation

We primarily collected the entire pharmacophore features based on MD-simulated of DBM peptide and crystal synthetic peptide ligands in complex with the Dvl PDZ domain (3CBX, 3CBY, and 3CC0) (Fig. 3a, b). To identify highly potent and diverse non-peptide small-molecule inhibitors blocking the Dvl–CXXC5 interaction, two different pharmacophore models, Pharm A and Pharm B, were generated based on two combinations of the entire pharmacophore features (Fig. 3c, d). Since the carboxylate-binding loop in the βB sheet recognized the peptide ligand C-terminus by serving as HBDs, the two HBAs (HBA 1 and HBA 2, Fig. 3a, b) were firstly considered.

It was confirmed that two hydrophobic features (HY 1 and HY 2, Fig. 3a, b) are critical features for Dvl PDZ domain inhibitors [13, 15] next to the carboxyl group. Additionally, H-bond interaction (HBA 3, Fig. 3a, b) with residue Arg325 in the αB helix-5′, specific to the Dvl PDZ domain, has been reported to be an estimation of binding specificity [28]. Therefore, HBA 1–3, HY 1, and HY 2 were included in both Pharm A and Pharm B models as common features (colored in orange, Fig. 3a).

The Pharm A model (Fig. 3c) incorporated two other hydrophobic interactions, HY 3 and HY 4. The HY 3 feature, which has been reported as a significant feature for Dvl PDZ binders [16], derived from the side chains of Arg of simulated DBM peptide (Fig. 2a, b) and Tyr of synthetic peptide ligands of complexes (3CBX and 3CBY, Fig. 2c). The HY 4 feature that was derived from the side chains of

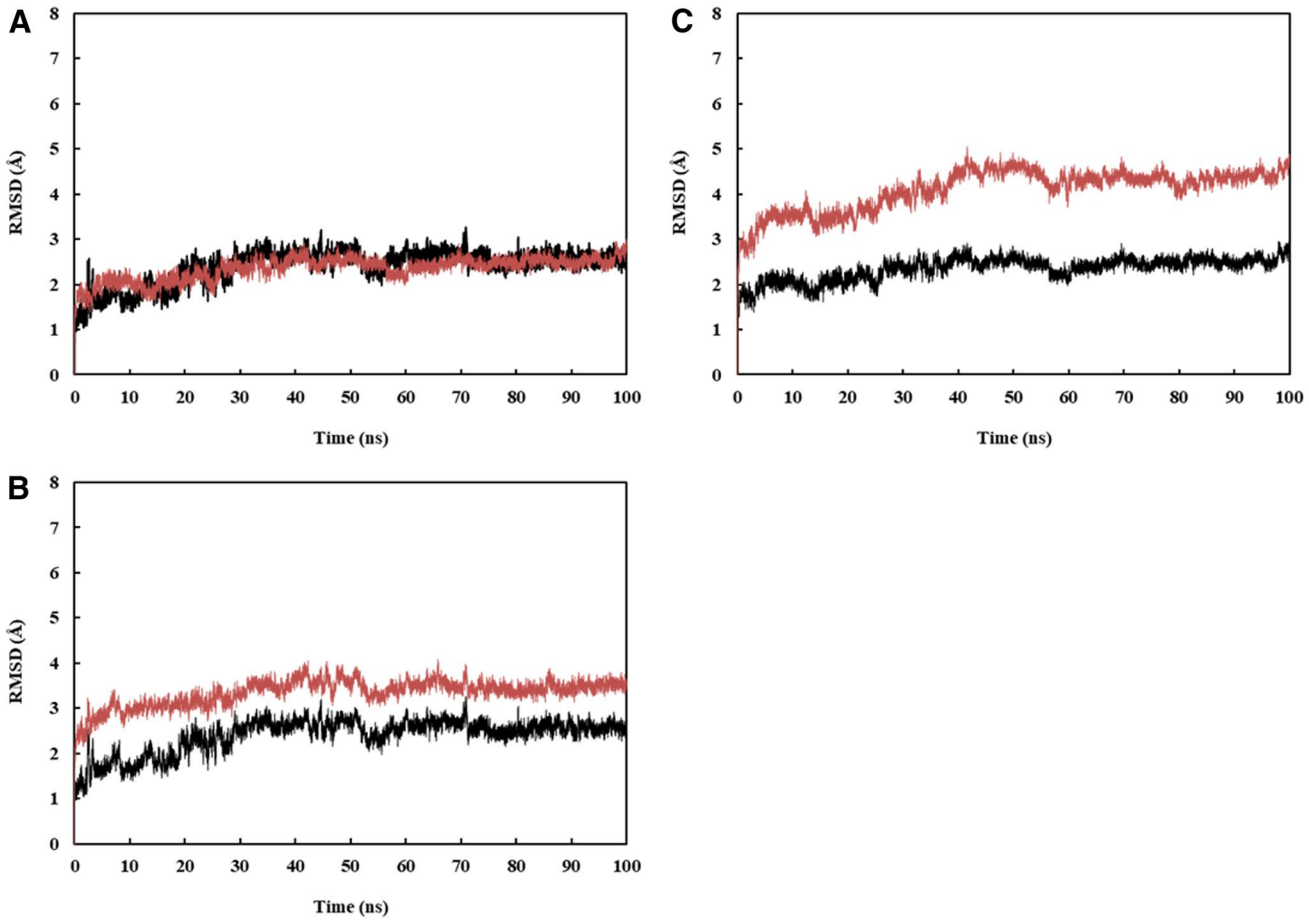

Fig. 1 RMSDs obtained from the MD systems during 100 ns explicit solvent simulations. **a** Backbone RMSD of the Dvl–DBM (red) and Dvl–Dapper (black) complexes obtained from the 100 ns MD simulations. **b** Sidechain RMSD (red) and backbone RMSD (black) of Dvl PDZ–Dapper peptide complexes during the 100 ns MD simulations. **c** Sidechain RMSD (red) and backbone RMSD (black) of Dvl PDZ–DBM peptide complexes during the 100 ns MD simulations

Lys in the simulated DBM peptide (Fig. 2a, b) and Trp of synthetic peptide of complex (3CBX, Fig. 2c), interacts with side chains of Ser265, Val267 residues in the βB sheet.

The Pharm B model (Fig. 3d) incorporated one hydrophobic feature (HY 5) and one HBD feature. The HY 5 feature derived from Ile and Pro residue at position + 1 of synthetic peptide ligand of complex (3CC0, Fig. 2d) was expected to interact with the side chain of Phe264 of the Dvl PDZ domain, which has been reported to be involved in increased binding affinity [13]. The HBD feature was derived from the amino group backbone of simulated DBM peptide (Fig. 2a, b) and synthetic peptide ligand of complex (3CC0, Fig. 2d) to form an H-bond with Ile269, which has an impact on the binding of inhibitors to the Dvl PDZ domain [15].

Pharmacophore-based virtual screening

The two pharmacophore models were used as 3D queries for retrieving potential inhibitors of Dvl–CXXC5 interaction from the integrated 3D database. As shown in Fig. 4, the Catalyst™ software package (DS) was used to identify compounds that fit to the pharmacophore models, and 1129 compounds and 346 compounds that showed good mapping with Pharm A and Pharm B (Fit value > 2.50), respectively, were chosen. After cluster analysis for further filtering, 10 and 6 compounds for Pharm A and Pharm B, respectively, were selected based on their structural similarities and differences. After visual inspection, 16 compounds (herein referred to as BMD4722 to BMD4737) were selected for experimental evaluation (Fig. 5).

Competitive Dvl–CXXC5 binding assay

The virtual hits were experimentally tested in the optimized sensitive and competitive fluorescence polarization binding system to identify small-molecule inhibitor of the Dvl–CXXC5 interaction. Fluorescence polarization can be monitored by the change in polarization of virtual hit

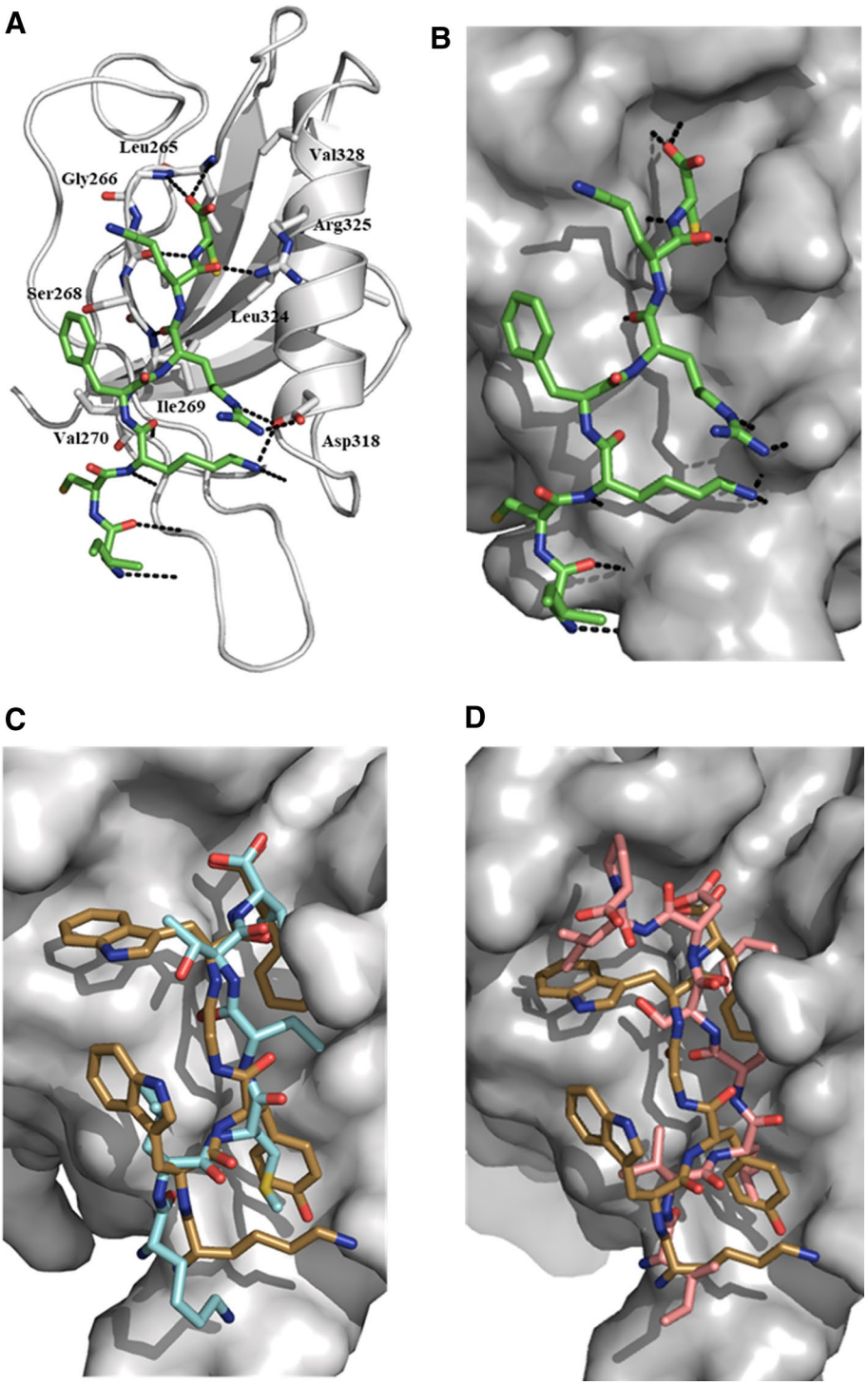

Fig. 2 Conformation of the DBM peptide docked into the PDZ domain and compared with crystal peptides. **a** Binding interactions of MD-simulated Dvl PDZ with the DBM peptide (green). The Dvl PDZ domain is in cartoon representation. **b** The Dvl PDZ domain is in surface representation. **c** Alignment of crystal Dapper peptide (cyan, 1L6O) and a synthetic peptide (sand, 3CBX); **d** Alignment of the two synthetic peptides (sand, 3CBX and salmon, 3CC0); the Dvl PDZ domain is in surface representation. Peptides are in stick representation. Figures were drawn with PyMOL software

compounds competing with the FITC-conjugated DBM peptide binding to the Dvl PDZ domain. Firstly, the virtual hit compounds were screened with fluorescence polarization at concentrations of 3, 10 and 30 μM. As shown in Fig. 6a, four out of 16 virtual hit compounds (BMD4722, BMD4724, BMD4726, and BMD4733) showed dose-dependent inhibitory effect and reduced the fluorescence intensities by 22.6, 40.8, 40.7, and 52.3%, respectively, of Dvl–CXXC5 interaction at 10 μM concentration. The four compounds were further tested in a dose–response experiment with fluorescence polarization at various concentrations (0.1, 1, 3, 10, 30, 50 and 100 μM) and IC_{50} values are shown in Fig. 6b. The IC_{50} values for 4 compounds (2.591, 0.149, 0.741, and 0.226 μM for BMD4722, BMD4724, BMD4726, and BMD4733,

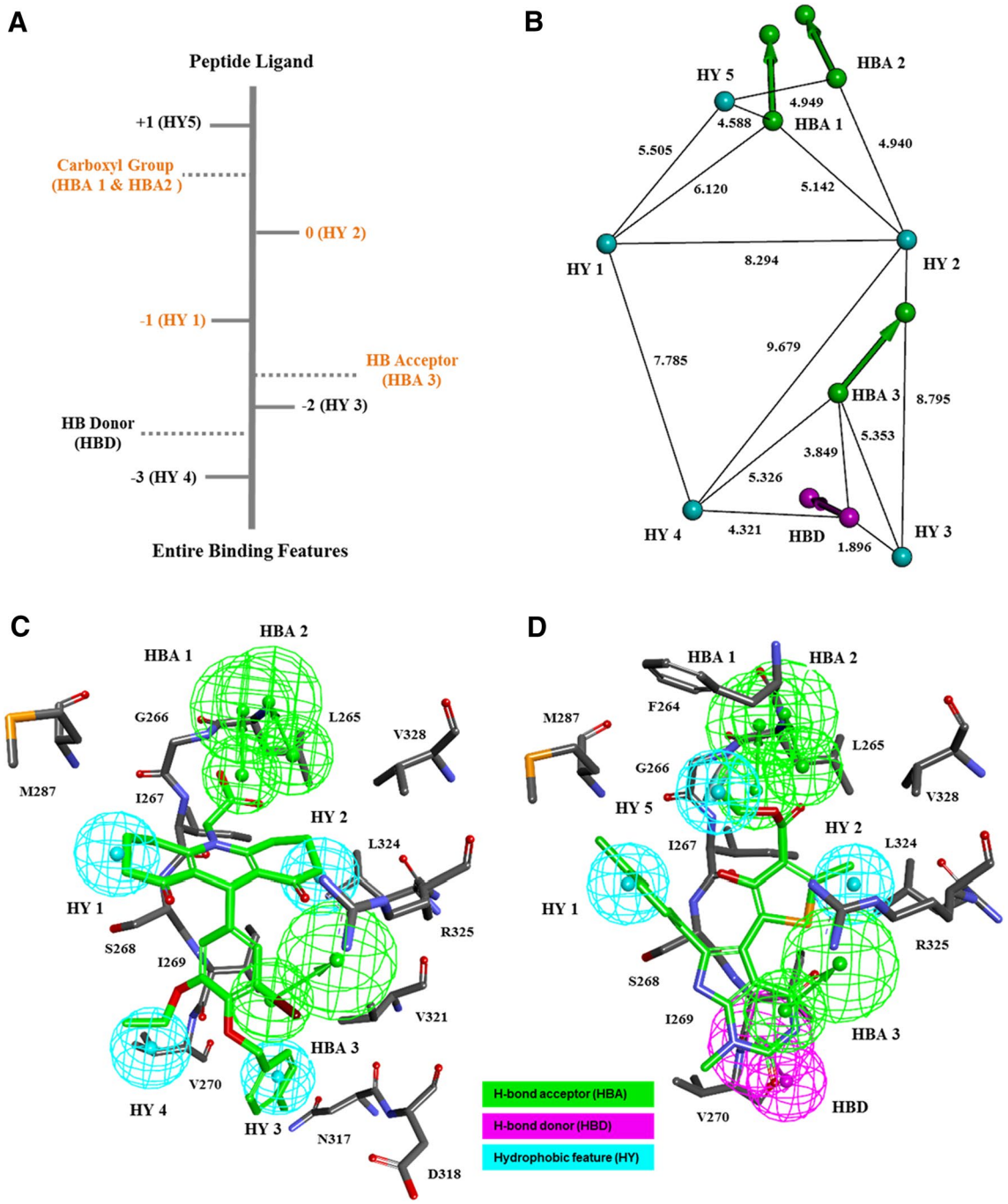

Fig. 3 Pharmacophore models for Dvl PDZ domain inhibitors. **a** Entire pharmacophoric features of Dvl PDZ domain-binding peptides contains 3 H-bond acceptors (HBAs), 1 H-bond donor (HBD) and 5 hydrophobic features (HYs). **b** Pharmacophoric feature distances without location constraints and between certain features, represented in Å. **c** Mapping of Pharm A representative virtual hit, BMD4722, onto the Pharm A model. **d** Mapping of Pharm B representative virtual hit, BMD4733, onto the Pharm B model. Features in the pharmacophore models are color coded: HBA in green; HBD in pink; and HY in cyan

respectively) were lower than 3 μM, suggesting that the four compounds effectively disrupted the interaction between Dvl PDZ domain and the DBM peptide. These results demonstrate that Dvl–CXXC5 interaction can be disrupted by these four compounds.

Binding studies of the Dvl PDZ domain with BMD4722

Fluorescence spectrophotometry experiment was implemented to verify the direct binding of compounds identified

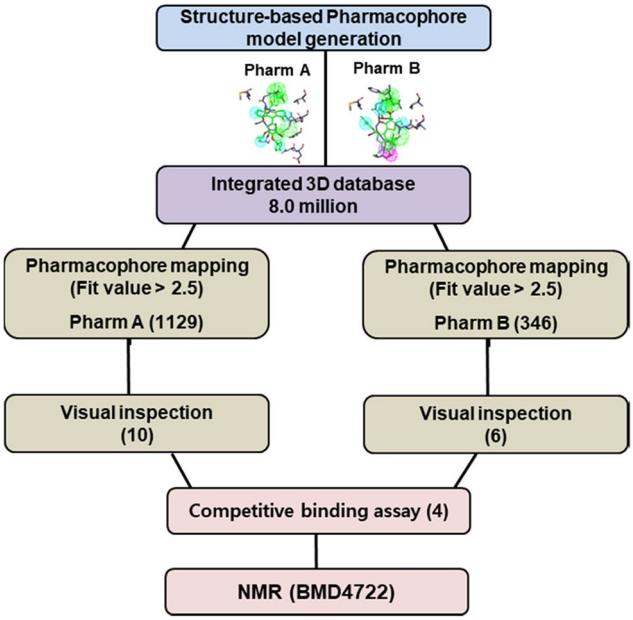

Fig. 4 Flow chart of the method used to discover small-molecule inhibitors of the Dvl PDZ domain

from competitive binding assay to the Dvl PDZ domain. The amount of BMD4722 was progressively increased to a molar ratio of 1:15 with the regular decrease of fluorescence intensity, indicating direct binding of BMD4722 to Dvl PDZ domain (Fig. 7). The K_D value of the Dvl PDZ–BMD4722 complex was calculated to be 22.3 μM. By contrast, BMD4724, BMD4726, and BMD4733 did not induce a change in fluorescence intensity, indicating an absence of interaction with the Dvl PDZ domain.

NMR and docking structure of Dvl PDZ–BMD4722 complex

To further investigate insights into the molecular determinants of Dvl PDZ domain and ligand interaction, which can be valuable for further ligand optimization, NMR chemical shift perturbation analysis (^{1}H–^{15}N-HSQC) and STD NMR were performed to examine evidence for the direct interaction of BMD4722 with the Dvl PDZ domain. NMR chemical shift perturbation experiment revealed the residues of the Dvl PDZ domain that interact with the ligand. The series of ^{1}H–^{15}N correlation spectra exhibited prominent chemical shift perturbations of Ile267, Ser268, Ile269, Val323, and Arg325 in the Dvl PDZ domain. Ile267, Ser268, Ile269 residues are in the βB sheet of the Dvl PDZ domain, and Val323 and Arg325 are in the αA helix (Fig. 8a–c). These results suggest that compound BMD4722 strongly interacts with Dvl PDZ binding site in a manner similar to that of the Dvl–CXXC5 interaction inhibitors, DBM, KY-02061, and KY-02327 [18]. In STD NMR, off-resonance (without protein saturation) signal intensities represented all protons associated with BMD4722. I_{STD} was obtained by subtracting on-resonance (with protein saturation) from off-resonance and revealed the functional group of the ligand that interacts with the Dvl PDZ domain. Six peaks of I_{STD} corresponding to 11 H atoms were easily distinguishable, as shown in Fig. 8d. The 11 H atoms were evenly distributed among the entire structure of compound BMD4722, which indicates that most parts of compound BMD4722 directly interact with the Dvl PDZ domain.

To determine the binding specificity, a docking study was implemented with the CDOCKER protocol in DS, and the binding pose was selected by considering the rank of calculated binding energies and results from ^{1}H–^{15}N-HSQC and STD NMR experiments. We found that the docked BMD4722 pose has a similar conformation to that of the simulated DBM–Dvl PDZ domain complex. In Fig. 9a, b, as expected from Pharm A, the carboxyl group (O4 and O5) of BMD4722 formed two H-bonds with the amide groups of Leu265 and Ile267 in the carboxylate-binding loop, as evidenced by the peaks at H-2′ in the STD NMR experiment. Instead of H-bonding interaction, the side chain of Arg325 neatly interacted with benzyl ring (C21-26) via a cation-π interaction, as evidenced by the peaks at H-22′ and H-26′ in the STD NMR experiment. Structure of the acridinedione group occupied the binding pockets at HY 1 and HY 2 feature of pharmacophore model simultaneously, coinciding with the peaks at H-13′and H-16′ in the STD NMR experiment. The phenyl group consisted of atoms C29, C32-37 totally occupied the binding pocket of HY 3 in the Pharm A model, identical to the peaks at H-32′, 33′, 35′, 36′, and H-37′ in the STD NMR experiment. Because HY 3-overlaid Arg in the DBM peptide interacted with Asp318 in αB-5′ by hydrogen bonding (Fig. 2a, b), adding a hydrogen bond donor to the phenyl group may increase the binding affinity. The ethoxy group occupied the binding pocket at HY 4 in the Pharm A model, as evidenced by the peaks at H-38′ and H-39′ in the STD NMR experiment. The flexible docking protocol implemented in DS was used as a double-check of BMD4722 binding mode, which provided a binding pose similar to that mentioned above. (Fig. S1 in supplementary file). Binding modes of BMD4724, BMD4726 and BMD4733 were also modeled by CDOCKER protocol in DS, compared with that of BMD4722 (Fig. S2 in supplementary file).

An additional MD was implemented to inspect stability of the interaction between Dvl PDZ domain and BMD4722 by using docking pose obtained from CDOCKER as the initial pose. As shown in Fig. 9c, the small RMSD fluctuation implied the stability of Dvl PDZ when bound to BMD4722. The movies composed of trajectory snapshot configurations (supplementary file) during the simulation shown that BMD4722 was

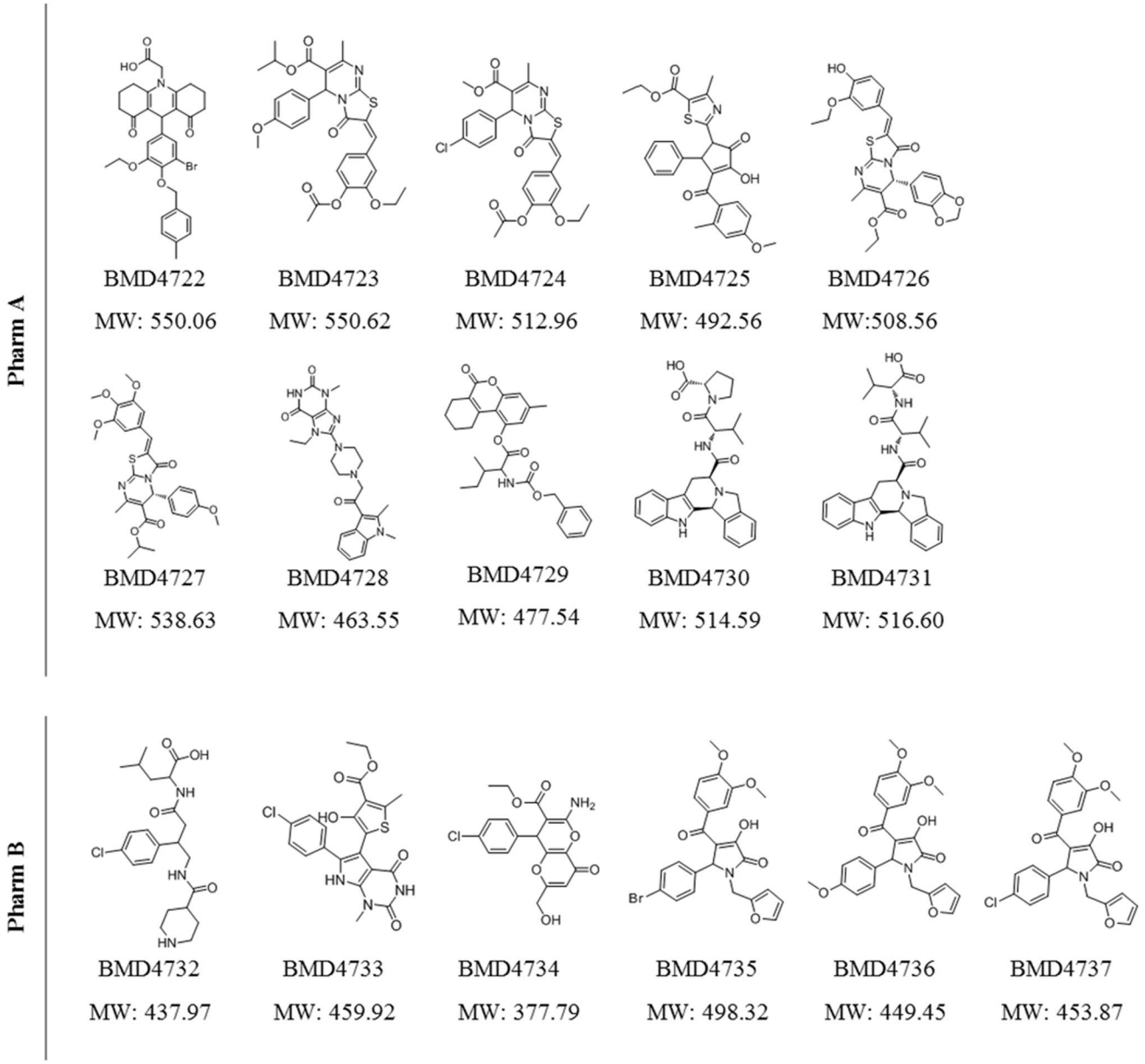

Fig. 5 Structures of 16 virtual hits screened through the pharmacophore models

trapped in the binding pocket of Dvl PDZ in water environment. Furthermore, the favorably interacting residues shown in Fig. 9d (Ile267, Ser268, Ile269, Arg325) are in good accord with the NMR chemical shift perturbation map of Dvl PDZ in BMD4722 chemical ligand titration (Fig. 8a). Interestingly, residue Arg325 in the αB helix-5′, which was reported as a significant interaction in previous papers [15, 16, 28], formed a water-mediated, rather than direct H-bond with BMD4722.

Discussion and conclusion

To identify inhibitors of PPI of Dvl PDZ and CXXC5, rather than selecting starting molecules from known inhibitors or binders, we set the specific interactions of Dvl PDZ and CXXC5 as the starting point to generate pharmacophore models. First, we conducted MD to simulate the interaction of the Dvl PDZ domain and CXXC5 peptide.

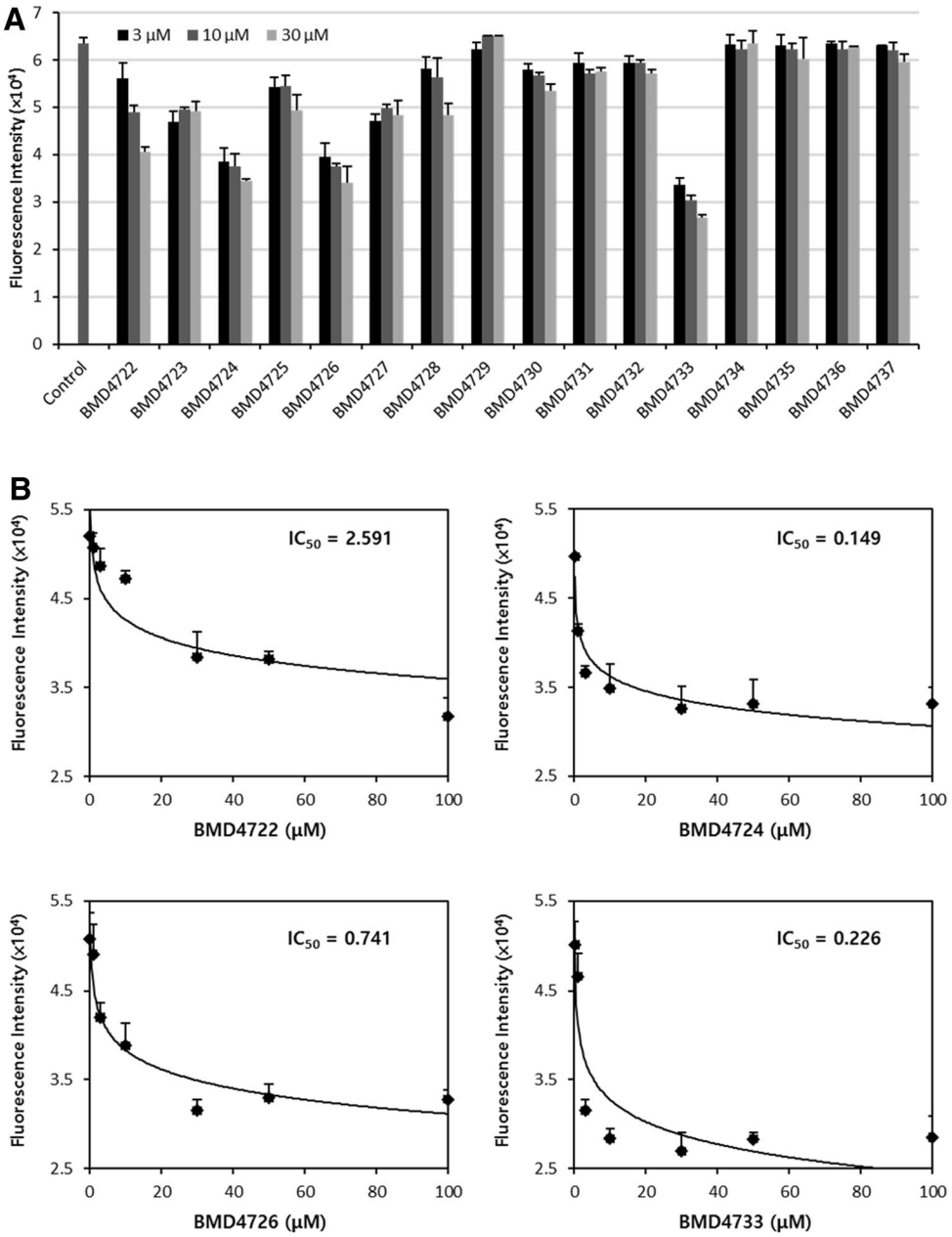

Fig. 6 Competitive binding analysis. **a** Screening results of 16 virtual hit compounds competing Dvl–CXXC5 interaction by competitive fluorescence polarization binding system. **b** Competition curves for the Dvl–CXXC5 interaction by the four compounds (BMD4722, BMD4724, BMD4726, and BMD4733)

Second, entire pharmacophore features were derived based on structural analysis of the MD-simulated DBM peptide-Dvl PDZ domain binding modes and crystal structures of the Dvl PDZ domain with synthetic peptide–ligands. Third, two combinations of pharmacophore features were selected to generate the pharmacophore models Pharm A and Pharm B. Subsequently, pharmacophore-based virtual screenings were performed, resulting in 16 virtual hit compounds for experimental validation.

Fluorescence polarization showed that four out of the 16 compounds effectively disrupted the Dvl–CXXC5 interactions; potential compounds were validated by fluorescence spectroscopy and NMR. Finally, the most potent Dvl–CXXC5 interaction inhibitor, BMD4722 from Pharm A, was found to directly bind to the Dvl PDZ domain and disrupt the Dvl–CXXC5 interaction. The binding mode of BMD4722 was modeled by docking study and the stability of the binding mode was validated by an additional MD simulation.

Pharm A contained all core pharmacophoric features identified in our previous study [16]. Differently, Pharm A increased the distances between core pharmacophoric features, particularly to the hydrophobic features (HY 1, HY 2 and HY 3), and added a new hydrophobic feature, HY 4. The geometry of three hydrophobic features appeared to be critical for interrupting the interaction of Dvl PDZ and CXXC5,

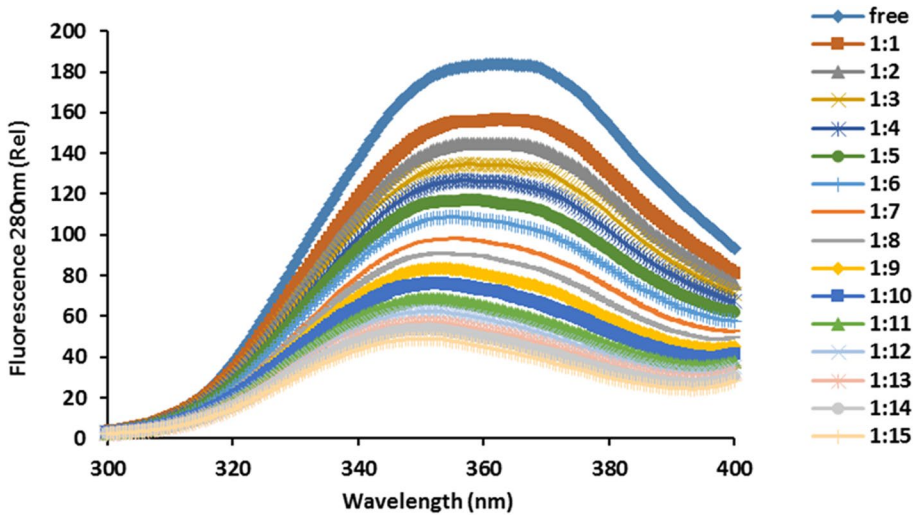

Fig. 7 Binding affinity of Dvl PDZ domain with BMD4722. Fluorescence spectroscopy indicates the binding affinity between Dvl PDZ and BMD4722. Titration between Dvl PDZ and BMD4722 was performed up to a molar ratios of 1:15, and the K_D value was calculated as 22.3 μM using Eq. 1

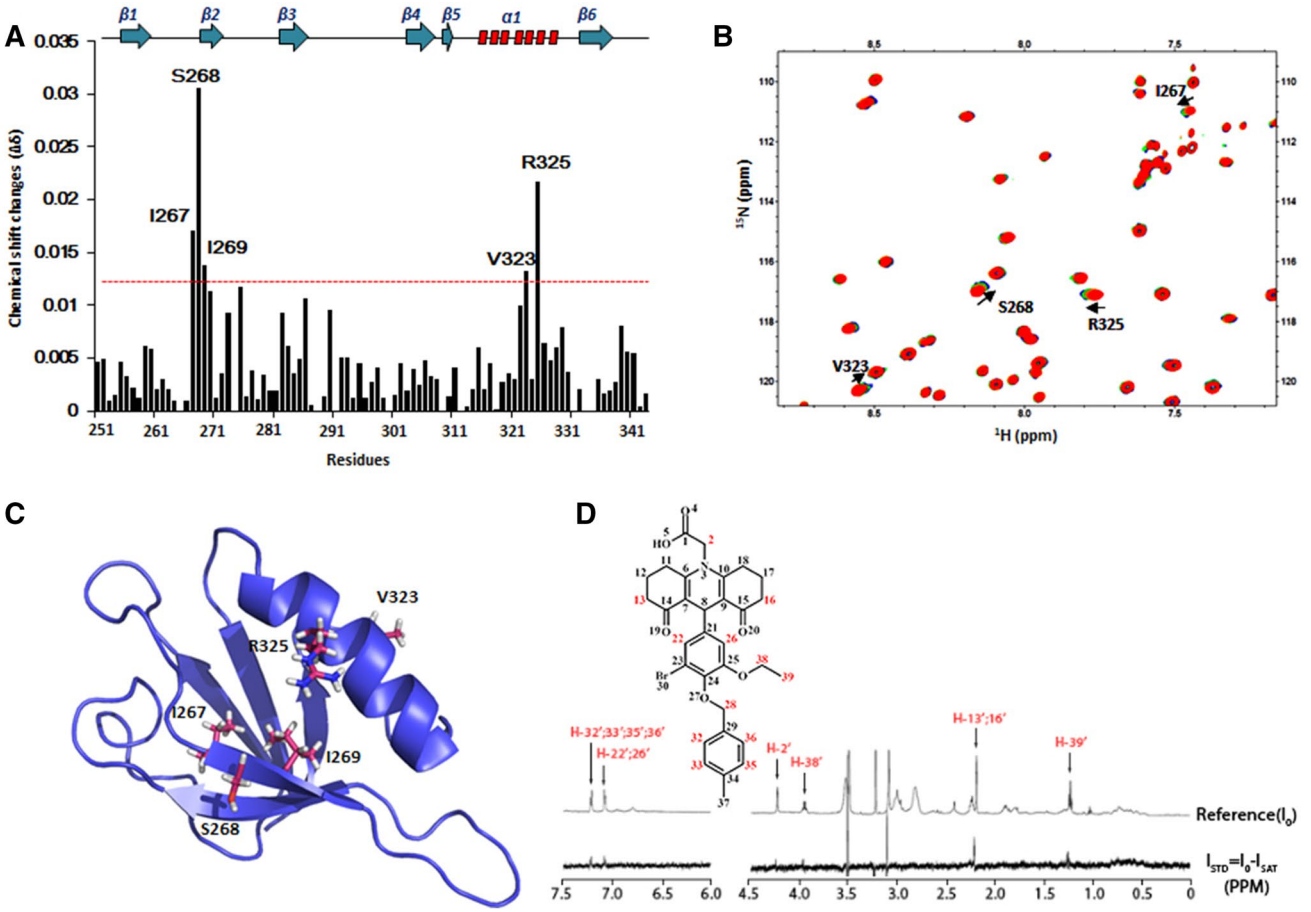

Fig. 8 Ligand binding site mapping on Dvl PDZ by NMR spectroscopy. **a** NMR chemical shift perturbation map of Dvl PDZ in BMD4722 chemical ligand titration. The bar diagram reveals the chemical shift changes at a Dvl PDZ–BMD4722 ligand molar ratio of 1:30. Three residues of βB and two residues of αB of Dvl PDZ are involved in BMD4722 chemical ligand interaction. **b** Overlay of ^{15}N–^{1}H HSQC spectra from NMR titration using the different protein/ligand molar ratios. ^{15}N-labeled Dvl-1 was titrated with BMD4722 chemical ligand. Different molar ratios of Dvl PDZ and BMD4722 ligand 1:0, 1:10, 1:20, and 1:30 are displayed as red, orange, green, and blue, respectively. **c** Main binding sites of the ligand are shown in stick representation (colored in magenta) based on chemical shift changes (Δδ) as described in A. **d** STD NMR spectrum recorded by selective saturation pulse. The resonances of functional proton in BMD4722 are indicated in the reference spectrum (I_0). Subtraction of saturation spectrum (I_{SAT}) from reference spectrum (I_0) results in I_{STD}. The incompletely suppressed water signal around 4.7 ppm was removed

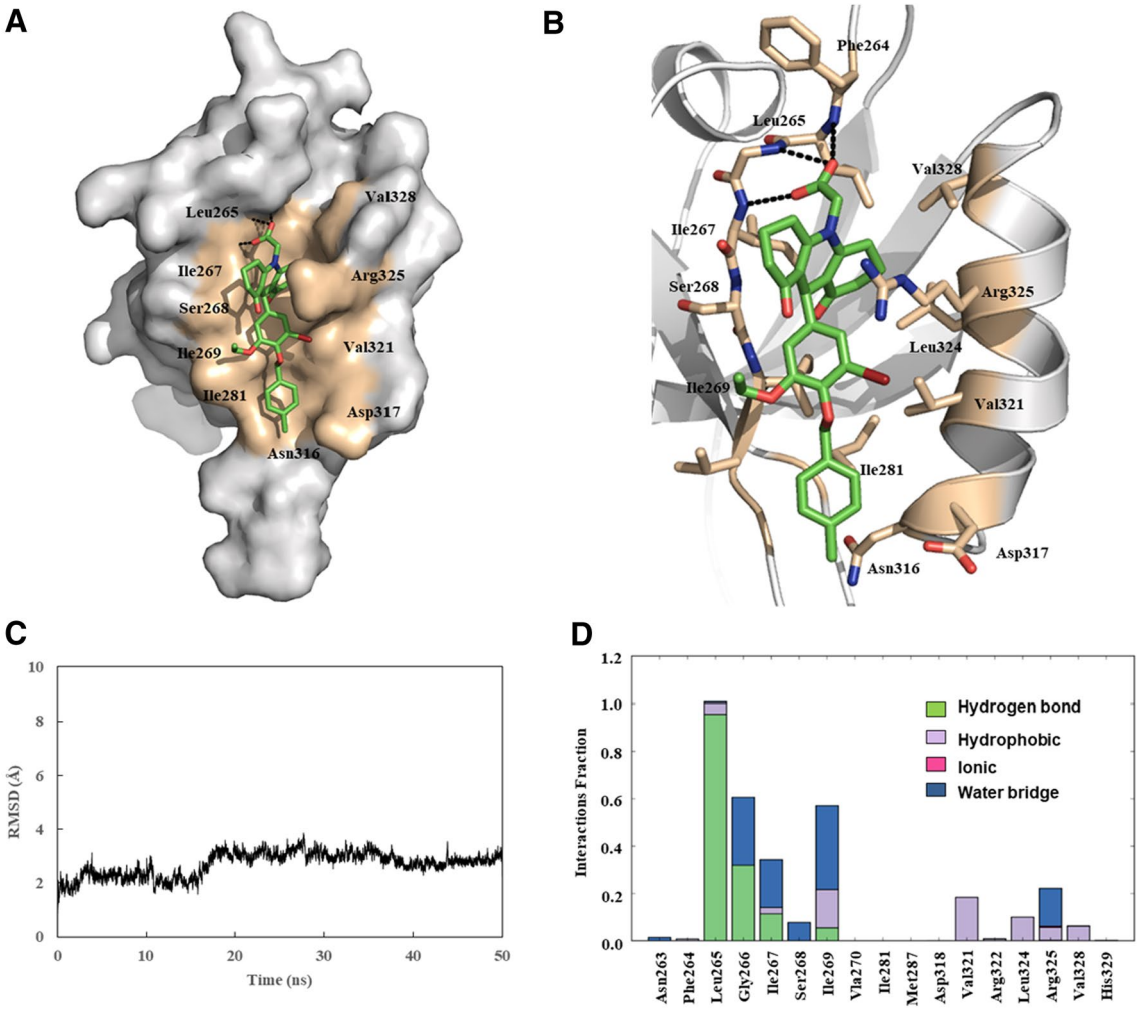

Fig. 9 Molecular docking simulation of Dvl PDZ–BMD4722 complex structure. **a** Binding interaction of molecular docking simulated BMD4722 (green) bound to the Dvl PDZ domain. The Dvl PDZ domain is in surface representation, the surfaces of residues that interact with BMD4722 are colored in red, and others are shown in gray. **b** Detailed interactions between BMD4722 and the Dvl PDZ domain. A and B were drawn with PyMOL software. **c** RMSD of the Dvl PDZ–BMD4722 (black line) complexes obtained from the MD simulations during 50 ns explicit solvent simulations. **d** Simulated protein–ligand interaction plot of Dvl PDZ domain and BMD4722. Stacked bar charts are normalized over the course of the trajectory, showing the percentages of four type interactions, hydrogen bonds, hydrophobic contacts, ionic interactions and water bridges

and alternating distances of core pharmacophoric feature may be a starting point for identifying specific inhibitors of Dvl PDZ induced PPIs.

In conclusion, the DBM–Dvl PDZ domain complex based pharmacophore combined with various traditional and simple computational approaches was used to identify the first potent representatives of a new class of inhibitors of the Dvl–CXXC5 interaction with an acridinedione scaffold. The potent inhibitor BMD4722 may be used as a template for further chemical optimization to design more potent and specific disruptors of Dvl–CXXC5 interaction.

Acknowledgements This work was supported by the Ministry of Knowledge Economy through Korea Research Institute of Chemical Technology (SI-1205, SI-1304, SI-1404), and Basic Science Research Program through the National Research Foundation of Korea (NRF) funded by the Ministry of Education (NRF-2016R1A6A3A04010213).

References

1. Long F (2012) Building strong bones: molecular regulation of the osteoblast lineage. Nat Rev Mol Cell Biol 13(1):27–38
2. Dees C, Distler JH (2013) Canonical Wnt signalling as a key regulator of fibrogenesis: implications for targeted therapies?. Exp Dermatol 22(11):710–713. https://doi.org/10.1111/exd.12255
3. Schinner S (2009) Wnt-signalling and the metabolic syndrome. Horm Metab Res 41(2):159–163. https://doi.org/10.1055/s-0028-1119408

4. Berwick DC, Harvey K (2012) The importance of Wnt signalling for neurodegeneration in Parkinson's disease. Biochem Soc Trans 40(5):1123–1128. https://doi.org/10.1042/bst20120122
5. Inestrosa NC, Montecinos-Oliva C, Fuenzalida M (2012) Wnt signaling: role in Alzheimer disease and schizophrenia. J Neuroimmune Pharmacol 7(4):788–807. https://doi.org/10.1007/s11481-012-9417-5
6. Rachner TD, Khosla S, Hofbauer LC (2011) Osteoporosis: now and the future. Lancet 377(9773):1276–1287. https://doi.org/10.1016/s0140-6736(10)62349-5
7. Regard JB, Zhong Z, Williams BO, Yang Y (2012) Wnt signaling in bone development and disease: making stronger bone with Wnts. Cold Spring Harb Perspect Biol. https://doi.org/10.1101/cshperspect.a007997
8. Ke HZ, Richards WG, Li X, Ominsky MS (2012) Sclerostin and Dickkopf-1 as therapeutic targets in bone diseases. Endocr Rev 33(5):747–783. https://doi.org/10.1210/er.2011-1060
9. Kim HY, Yoon JY, Yun JH, Cho KW, Lee SH, Rhee YM, Jung HS, Lim HJ, Lee H, Choi J, Heo JN, Lee W, No KT, Min D, Choi KY (2015) CXXC5 is a negative-feedback regulator of the Wnt/[beta]-catenin pathway involved in osteoblast differentiation. Cell Death Differ 22(6):912–920. https://doi.org/10.1038/cdd.2014.238
10. Andersson T, Södersten E, Duckworth JK, Cascante A, Fritz N, Sacchetti P, Cervenka I, Bryja V, Hermanson O (2009) CXXC5 Is a Novel BMP4-regulated modulator of Wnt signaling in neural stem cells. J Biol Chem 284(6):3672–3681. https://doi.org/10.1074/jbc.M808119200
11. Kim MS, Yoon SK, Bollig F, Kitagaki J, Hur W, Whye NJ, Wu YP, Rivera MN, Park JY, Kim HS, Malik K, Bell DW, Englert C, Perantoni AO, Lee SB (2010) A novel Wilms tumor 1 (WT1) target gene negatively regulates the WNT signaling pathway. J Biol Chem 285(19):14585–14593. https://doi.org/10.1074/jbc.M109.094334
12. Knappskog S, Myklebust LM, Busch C, Aloysius T, Varhaug JE, Lonning PE, Lillehaug JR, Pendino F (2011) RINF (CXXC5) is overexpressed in solid tumors and is an unfavorable prognostic factor in breast cancer. Ann Oncol 22(10):2208–2215. https://doi.org/10.1093/annonc/mdq737
13. Shan J, Shi DL, Wang J, Zheng J (2005) Identification of a specific inhibitor of the dishevelled PDZ domain. Biochemistry 44(47):15495–15503. https://doi.org/10.1021/bi0512602
14. Grandy D, Shan J, Zhang X, Rao S, Akunuru S, Li H, Zhang Y, Alpatov I, Zhang XA, Lang RA, Shi DL, Zheng JJ (2009) Discovery and characterization of a small molecule inhibitor of the PDZ domain of dishevelled. J Biol Chem 284(24):16256–16263. https://doi.org/10.1074/jbc.M109.009647
15. Shan J, Zheng JJ (2009) Optimizing Dvl PDZ domain inhibitor by exploring chemical space. J Comput-Aided Mol Des 23(1):37–47. https://doi.org/10.1007/s10822-008-9236-1
16. Choi J, Ma S, Kim H-Y, Yun J-H, Heo J-N, Lee W, Choi K-Y, No KT (2016) Identification of small-molecule compounds targeting the dishevelled PDZ domain by virtual screening and binding studies. Bioorg Med Chem 24(15):3259–3266. https://doi.org/10.1016/j.bmc.2016.03.026
17. Fujii N, You L, Xu Z, Uematsu K, Shan J, He B, Mikami I, Edmondson LR, Neale G, Zheng J, Guy RK, Jablons DM (2007) An antagonist of dishevelled protein-protein interaction suppresses β-catenin–dependent tumor cell growth. Can Res 67(2):573–579. https://doi.org/10.1158/0008-5472.can-06-2726
18. Kim HY, Choi S, Yoon JH, Lim HJ, Lee H, Choi J, Ro EJ, Heo JN, Lee W, No KT, Choi KY (2016) Small molecule inhibitors of the Dishevelled-CXXC5 interaction are new drug candidates for bone anabolic osteoporosis therapy. EMBO Mol Med. https://doi.org/10.15252/emmm.201505714
19. Shivakumar D, Williams J, Wu Y, Damm W, Shelley J, Sherman W (2010) Prediction of absolute solvation free energies using molecular dynamics free energy perturbation and the OPLS force field. J Chem Theory Comput 6(5):1509–1519. https://doi.org/10.1021/ct900587b
20. Guo Z, Mohanty U, Noehre J, Sawyer TK, Sherman W, Krilov G (2010) Probing the α-helical structural stability of stapled p53 peptides: molecular dynamics simulations and analysis. Chem Biol Drug Des 75(4):348–359. https://doi.org/10.1111/j.1747-0285.2010.00951.x
21. Bowers KJ, Chow E, Xu H, Dror RO, Eastwood MP, Gregersen BA, Klepeis JL, Kolossvary I, Moraes MA, Sacerdoti FD, Salmon JK, Shan Y, Shaw DE (2006) Scalable algorithms for molecular dynamics simulations on commodity clusters. In: Proceedings of the ACM/IEEE Conference on Supercomputing (SC06), Tampa, Florida, November 11–17
22. Jorgensen WL, Chandrasekhar J, Madura JD, Impey RW, Klein ML (1983) Comparison of simple potential functions for simulating liquid water. J Chem Phys 79(2):926–935. https://doi.org/10.1063/1.445869
23. Essmann U, Perera L, Berkowitz ML, Darden T, Lee H, Pedersen LG (1995) A smooth particle mesh Ewald method. J Chem Phys 103(19):8577–8593. https://doi.org/10.1063/1.470117
24. Hoover WG (1985) Canonical dynamics: equilibrium phase-space distributions. Phys Rev A 31(3):1695–1697
25. Martyna GJ, Tobias DJ, Klein ML (1994) Constant pressure molecular dynamics algorithms. J Chem Phys 101(5):4177–4189. https://doi.org/10.1063/1.467468
26. Humphreys DD, Friesner RA, Berne BJ (1994) A multiple-time-step molecular dynamics algorithm for macromolecules. J Phys Chem 98(27):6885–6892. https://doi.org/10.1021/j100078a035
27. Schrodinger LLC (2010) The PyMOL molecular graphics system, version 1.3r1
28. Lee HJ, Wang NX, Shi DL, Zheng JJ (2009) Sulindac inhibits canonical Wnt signaling by blocking the PDZ domain of the protein Dishevelled. Angew Chem Int Ed 48(35):6448–6452. https://doi.org/10.1002/anie.200902981